AIMS Mathematics, 8(3): 5789–5815.
DOI: 10.3934/math.2023292
Received: 10 October 2022
Revised: 15 November 2022
Accepted: 28 November 2022
Published: 26 December 2022

http://www.aimspress.com/journal/Math

Research article

A class of HOC finite difference method for elliptic interface problems with imperfect contact

Fujun Cao[1,2,*] **and Dongfang Yuan**[1,2]

[1] School of Science, Inner Mongolia University of Science and Technology, Baotou, China
[2] School of Mathematics and Science, Inner Mongolia Normal University, Hohhot, China

* **Correspondence:** Email: caofujun@imust.edu.cn.

Abstract: The elliptic interface problems with imperfect contact have found applications in numerical solutions of the Stefan problem of the solidification process and crystal growth, composite materials, multi-phase flows, etc. In this paper a 1D elliptic interface problem with imperfect contact is considered. A class of high-order compact finite difference schemes are constructed on body-fitted and non-body-fitted mesh, respectively. For each case, the second-, third- and fourth-order approximations of implicit jump conditions are provided by using the jump conditions and its high-order derivatives. Numerical examples are provided to verify the performance of the schemes. The numerical results demonstrate that the schemes have theoretical accuracy for elliptic interface problems with imperfect contact.

Keywords: implicit jump conditions; elliptic interface problem; imperfect contact; sharp interface
Mathematics Subject Classification: 35J40, 35R05

1. Introduction

A class of problems that give rise of singular behavior are elliptic interface problems with imperfect contact [1], and it is featured by the implicit jump condition imposed on the imperfect contact interface, and the jumping quantity of the unknown is related to the flux across the interface. The elliptic interface problems with imperfect contact have been applied to model the Stefan problem of the solidification process and crystal growth, composite materials, multi-phase flows [2, 3] and the problem of temperature discontinuity between the gas and cooling solid surface [4]. More examples include the heat conduction between materials of the different heat capacities and conductivities and interface diffusion processes [5, 6], the temperature discontinuity between a gas and cooling solid surface [4], the conjugate heat transfer problem in thermodynamic processes between materials that are thermally coupled through non-adiabatic contacts [7], etc.

We consider the one-dimensional (1D) elliptic interface problem with imperfect contact

$$\begin{cases} -(\beta(x)u_x)_x + c(x)u = f(x), \quad x \in (0,\alpha) \cup (\alpha,1), \\ u(0) = u_0, \quad u(1) = u_1, \end{cases} \tag{1.1}$$

together with the following implicit jump conditions across the interface α

$$\begin{cases} [u] = u^+ - u^- = \lambda\beta^+\nabla u^+ \cdot \vec{n}, \\ [\beta\frac{\partial u}{\partial \vec{n}}] = 0, \end{cases} \tag{1.2}$$

where $0 < \alpha < 1$, $\vec{n}$ is a unit normal to the interface pointing from Ω^- to Ω^+. $g^\pm$ denotes the right and left limits of the function g at the point α, and $[g] = g^+ - g^-$. Without loss of generality, we assume that Ω is computational domain, and the interface α separates Ω into two sub-domains Ω^- and Ω^+.

The solution of the elliptic interface problems is often discontinuous due to discontinuous coefficients or singular sources across the interface. To recover the numerical accuracy near the interface, a variety of methods have been developed via enforcing the jump conditions (1.2) and (1.1) into numerical discretization such that accurate and robust numerical algorithms can be designed. Finite difference methods (FDMs) constitute a commonly used approach for elliptic interface problems. Since the publication of the original immersed interface method (IIM) [8], they have been applied to various problems, such as the Stokes flow with elastic boundaries or surface tension [9], incompressible flow based on the Navier-Stokes equations with singular source terms [10], and nonlinear problems in magneto-rheological fluids [11]. Many further developments and analysis in various aspects of the FDM for elliptic interface problems were carried out to improve the accuracy, stability or efficiency [12–19]. Many other elegant methods have been proposed in the past decade, including the ghost fluid method [20, 21], finite volume method [7, 22–24], the matched interface and boundary (MIB) method [25–27], etc. Finite element methods (FEMs) constitute another common practice to resolve the elliptic interface problems. With the help of body-fitted unstructured meshes, FEMs [28–30] have been developed for handling elliptic interfaces and irregular geometries. For interfaces with complex topologies, the construction of high quality body-fitted meshes could be difficult and time-consuming. This motivates the development of immersed FEMs based on non-body-fitted structured meshes [31–38], etc. Nevertheless, most interface schemes in the literatures are designed to be of second-order accuracy.

The strategy for generating higher-order difference schemes can be roughly divided into two categories. (1) The first category is expanding the stencil and including more points in the schemes [15, 16, 25–27, 39–42]. Advantages of this approaches is achieving high-order accuracy and using lower order jump conditions only. The obvious disadvantages of such approach is creating large matrix bandwidths and complicating the numerical treatment near the boundaries. Gibou and Fedkiw [16] introduced an $O(h^4)$ accurate finite difference discretization for the Laplace and heat equations on an irregular domain. Previous scholars [25–27] presented high-order MIB methods for solving elliptic equations with discontinuous coefficients and singular sources on Cartesian grids. This type of method is based on the use of fictitious points to achieve high-order accuracy. Zhong [40] presented a high-order IIM with general jump conditions by employing fictitious points to achieve high-order accuracy and using lower-order jump conditions only. Similar to the MIB approach, a wide stencil with more points are involved at irregular points. Feng and Zhao [42] introduced a new

Cartesian grid FDM based on the fourth-order accurate MIB method. Colnago et al. [15] presented a high-order IIM for solving Poisson equations with discontinuous coefficients on Cartesian grids, it combines the FDM and ghost node strategy and requires only the ordinary jumps of the function. (2) The second category involves using the differential equation and the interface relations as additional identities [13, 39, 41]. The advantage of this approach is that the scheme is compact and minimal stencil is used. The disadvantage is that to maintain high-order accuracy, it requires the knowledge of jump conditions of high-order derivatives. Li and Ito [13] constructed a fourth-order IIM by computing high-order jump conditions involving mixed derivatives. Linnick and Fasel [39] presented a high-order IIM for simulating unsteady incompressible flow in an irregular domain. Instead of using analytical jump conditions, they compute the jump conditions for higher derivatives numerically. Angelova and Vulkov [41] presented high-order compact FDM for elliptic equations with intersecting interfaces by using the differential equation and the jump (interface) relations as additional identities, which can be differentiated to eliminate higher-order local truncation errors. For FEMs, the higher-order convergence crucially depends on how well the interface is resolved by the triangular mesh. In practice, subparametric, isoparametric or superparametric elements are usually employed to secure the optimal order of $p + 1$ in the L_2 norm for a polynomial order of p, for both continuous [33, 43] and discontinuous Galerkin [34, 35, 44–46] FEMs. It is worth pointing out that most of the numerical methods in literatures are aimed at the elliptical interface problem with homogeneous jump conditions ($[u] = 0, [\beta u_{\vec{n}}] = 0$) or nonhomogeneous jump conditions where the jumps of the temperature as well as the conductive heat flux along the interface are known explicitly (say $[u] = g_1$, $[\beta\partial u/\partial\vec{n}] = g_2$, with known g_1 and g_2). When the elliptic interface problem has an implicit jump condition as in (1.2), there are comparatively few numerical methods for solving such problems.

In this paper, we consider the 1D elliptic interface problems with imperfect contact, where the implicit jump condition is a setting for the interface and the jump of the primary variable is proportional to the normal flux across the interface. A class of high-order FDMs is constructed for the 1D elliptic interface for both the body-fitted and non-body-fitted mesh. For each case, the second-, third- and fourth-order approximations of the implicit jump condition are provided by using the original variables on both sides of the interface and a set of jump conditions and its high order derivatives. Numerical examples are presented to verify the performance of the scheme. The numerical results show that the presented schemes can reach the theoretical accuracy for solving the elliptic interface problems with imperfect contact.

The rest of this paper is organized as follows. In Section 2, we formulate the scheme for 1D elliptic equations with imperfect interfaces. Section 3 constructs the approximation of the normal derivative for the interface. Section 4 computes the primary variables u^+ and u^- for the interface. Numerical examples are provided in Section 5 to demonstrate the accuracy and stability of the presented scheme. A concluding remark is given in Section 6.

2. High-order compact difference scheme

We assume that $\beta(x)$ in (1.1) is a piecewise smooth function with a jump at the interface α, and that $\beta(x)$ has upper and lower boundries:

$$0 < \beta_{min} \le \beta(x) \le \beta_{max}, \tag{2.1}$$

where β_{min} and β_{max} are two constants. The source term $f(x)$ is piecewise smooth.

Introduce a uniform grid $x_i = ih, i = 0, 1, \cdots, n$ with $h = \frac{1}{n}$. The fourth-order compact difference scheme is constructed and three-point computational stencil for each point is adopted. For node i, the three points in computational stencil are $\{x_{i-1}, x_i, x_{i+1}\}$. Without loss of generality, assume the interface α is located in a grid interval, $x_k \le \alpha \le x_{k+1}$. Because of the interface is located in the stencil, the points k and $k+1$ are named as irregular points, and $i \ne k, k+1$ are name as regular points.

At a regular point i, i.e., $i \ne k, k+1$, for convenience, we briefly give the construction process of the fourth order compact difference scheme, for more detailed information one can refer to Ref. [47].

$$-\beta\delta_x^2 u_i - \beta_x \delta_x u_i + c_i u_i + \tau = f_i, \tag{2.2}$$

where

$$\delta_x^2 u_i = \frac{u_{i+1} - 2u_i + u_{i-1}}{h^2}, \quad \delta_x u_i = \frac{u_{i+1} - u_{i-1}}{2h},$$

and

$$\tau = \beta_x \frac{h^2}{3!}\frac{\partial^3 u}{\partial x^3}\Big|_i + \beta \frac{h^2}{12}\frac{\partial^4 u}{x^4}\Big|_i + O(h^4).$$

Dropping the term τ in (2.2), it is the standard second-order central difference scheme. In order to get fourth-order scheme, we have to handle the high-order derivative terms $\frac{\partial^3 u}{\partial x^3}$ and $\frac{\partial^4 u}{\partial x^4}$. According to the governing equation (1.1), there is

$$u_{xx} = \frac{1}{\beta}(-\beta_x u_x + cu - f). \tag{2.3}$$

Taking the first and second derivatives to (2.3) respectively , we have

$$u_{xxx} = \phi_1 u_{xx} + \phi_2 u_x + \phi_3 u + \phi_4 f + \phi_5 f_x, \tag{2.4}$$

and

$$u_{xxxx} = \psi_1 u_{xx} + \psi_2 u_x + \psi_3 u + \psi_4, \tag{2.5}$$

where

$$\begin{aligned}
&\phi_1 = -\frac{\beta_x}{\beta}, \quad \phi_2 = \frac{\beta_x^2}{\beta^2} - \frac{\beta_{xx}}{\beta} + \frac{c}{\beta}, \quad \phi_3 = -\frac{c\beta_x}{\beta^2}, \quad \phi_4 = \frac{\beta_x}{\beta^2}, \quad \phi_5 = -\frac{1}{\beta},\\
&\psi_1 = \phi_1^2 + \phi_{1,x} + \phi_2, \quad \psi_2 = \phi_1\phi_2 + \phi_{2,x} + \phi_3, \quad \psi_3 = \phi_1\phi_3 + \phi_{3,x},\\
&\psi_4 = (\phi_1\phi_4 + \phi_{4,x})f + (\phi_1\phi_5 + \phi_4 + \phi_{5,x})f_x + \phi_5 f_{xx},\\
&\phi_{1,x} = \frac{\beta_x^2 - \beta\beta_{xx}}{\beta^2}, \quad \phi_{2,x} = 2\frac{\beta_x}{\beta}\frac{\beta\beta_{xx} - \beta^2}{\beta^2} - \frac{\beta\beta_{xxx} - \beta_x\beta_{xx}}{\beta^2} - \frac{c\beta_x}{\beta^2},\\
&\phi_{3,x} = \frac{c(2\beta_x^2 - \beta\beta_{xx})}{\beta^3}, \quad \phi_{4,x} = \frac{\beta\beta_{xx} - 2\beta_x^2}{\beta^3}, \quad \phi_{5,x} = \frac{\beta_x}{\beta^2}.
\end{aligned}$$

Substituting (2.4) and (2.5) into (2.2) and approximating the first- and second-derivatives with the central difference, we can get the fourth-order compact scheme:

$$A_i u_{i+1} + B_i u_i + C_i u_{i-1} = F_i + O(h^4), \tag{2.6}$$

where

$$A_i = \frac{-\beta + \phi_1\beta_x\frac{h^2}{6} + \psi_1\beta\frac{h^2}{12}}{h^2} + \frac{-\beta_x + \phi_2\beta_x\frac{h^2}{6} + \psi_2\beta\frac{h^2}{12}}{2h},$$
$$B_i = 2\frac{-\beta + \phi_1\beta_x\frac{h^2}{6} + \psi_1\beta\frac{h^2}{12}}{h^2} + (c + \phi_3\beta_x\frac{h^2}{6} + \psi_3\beta\frac{h^2}{12}),$$
$$C_i = \frac{-\beta + \phi_1\beta_x\frac{h^2}{6} + \psi_1\beta\frac{h^2}{12}}{h^2} - \frac{-\beta_x + \phi_2\beta_x\frac{h^2}{6} + \psi_2\beta\frac{h^2}{12}}{2h},$$
$$F_i = f_i - \beta_x\frac{h^2}{6}(\phi_4 f_i + \phi_5 f_{x,i}) - \beta\frac{h^2}{12}\psi_4.$$

2.1. *Interface fitted with mesh*

When the interface is in contact with one of the mesh nodes, it is referred to as the body-fitted case. Without loss of generality, we assume that the interface is located the mesh node k, as shown in Figure 1.

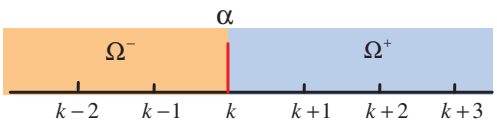

Figure 1. Interface fitted with body.

In this case, the irregular nodes are $k-1$ and $k+1$, and the compact stencil of these two irregular nodes are shown in Figure 2. Then, the high order compact scheme at these two irregular nodes can be given as

$$\bar{A}_{k-1}u_{k-2} + \bar{B}_{k-1}u_{k-1} + \bar{C}_{k-1}u^- = \bar{F}_{k-1}, \tag{2.7}$$

and

$$\bar{A}_{k+1}u^+ + \bar{B}_{k+1}u_{k+1} + \bar{C}_{k+1}u_{k+2} = \bar{F}_{k+1}. \tag{2.8}$$

Apparently, there are two auxiliary qualities u^- and u^+ in the schemes. To apply the above scheme, it is necessary to approximate the u^- and u^+ with adequate accuracy. We prepare to use the interface jump connecting conditions and establish the linear systems with u^+ and u^- as variables. The difficulty lies in the high-order discretization of the first-order derivatives u_x^+ and u_x^- on both sides of the interface.

$$\begin{cases} [u] = \lambda\beta^+ u_x^+, \\ [\beta u_{\vec{n}}] = 0. \end{cases} \tag{2.9}$$

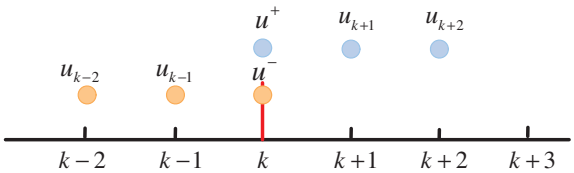

Figure 2. Irregular point stencil for interface-fitted mesh.

Expand the u_{k+1} and u_{k-1} at the interface α by using the Taylor series, it reads

$$\begin{aligned} u_{k+1} &= u^+ + h\frac{\partial u}{\partial x}\Big|^+ + \frac{h^2}{2!}\frac{\partial^2 u}{\partial x^2}\Big|^+ + \frac{h^3}{3!}\frac{\partial^3 u}{\partial x^3}\Big|^+ + \frac{h^4}{4!}\frac{\partial^4 u}{\partial x^4}\Big|^+ \\ &+ \frac{h^5}{5!}\frac{\partial^5 u}{\partial x^5}\Big|^+ + O(h^6), \end{aligned} \tag{2.10}$$

and

$$\begin{aligned} u_{k-1} &= u^- - h\frac{\partial u}{\partial x}\Big|^- + \frac{h^2}{2!}\frac{\partial^2 u}{\partial x^2}\Big|^- - \frac{h^3}{3!}\frac{\partial^3 u}{\partial x^3}\Big|^- + \frac{h^4}{4!}\frac{\partial^4 u}{\partial x^4}\Big|^- \\ &- \frac{h^5}{5!}\frac{\partial^5 u}{\partial x^5}\Big|^- + O(h^6). \end{aligned} \tag{2.11}$$

Rewritting the above two formulas, we can get the representations of $\frac{\partial u}{\partial x}\Big|^+$ and $\frac{\partial u}{\partial x}\Big|^-$ as follows

$$\begin{aligned} \frac{\partial u}{\partial x}\Big|^+ &= \frac{u_{k+1} - u^+}{h} - \frac{h}{2!}\frac{\partial^2 u}{\partial x^2}\Big|^+ - \frac{h^2}{3!}\frac{\partial^3 u}{\partial x^3}\Big|^+ - \frac{h^3}{4!}\frac{\partial^4 u}{\partial x^4}\Big|^+ \\ &- \frac{h^4}{5!}\frac{\partial^5 u}{\partial x^5}\Big|^+ + O(h^5), \end{aligned} \tag{2.12}$$

$$\begin{aligned} \frac{\partial u}{\partial x}\Big|^- &= \frac{u^- - u_{k-1}}{h} + \frac{h}{2!}\frac{\partial^2 u}{\partial x^2}\Big|^- - \frac{h^2}{3!}\frac{\partial^3 u}{\partial x^3}\Big|^- + \frac{h^3}{4!}\frac{\partial^4 u}{\partial x^4}\Big|^- \\ &- \frac{h^4}{5!}\frac{\partial^5 u}{\partial x^5}\Big|^- + O(h^5). \end{aligned} \tag{2.13}$$

According to the governing equation, we have

$$u^+_{xx} = \frac{1}{\beta^+}(-\beta^+_x u^+_x + c^+u^+ - f^+), \quad u^-_{xx} = \frac{1}{\beta^-}(-\beta^-_x u^-_x + c^-u^- - f^-). \tag{2.14}$$

Keeping the first two terms on the right-hand side of (2.12) and substituting (2.14) into (2.12), the second-order accurate approximate scheme of $\frac{\partial u}{\partial x}\Big|^+$ can be given as

$$\frac{\partial u}{\partial x}\Big|^+ = \rho_{r,1}u^+ + \rho_{r,2}u_{k+1} + \rho_{r,3} + O(h^2), \tag{2.15}$$

where

$$\rho_{r,1} = -(\frac{1}{h} + \frac{h}{2}\frac{c^+}{\beta^+})\Big/D_r, \quad \rho_{r,2} = \frac{1}{h}\Big/D_r, \quad \rho_{r,3} = \frac{h}{2}\frac{f^+}{\beta^+}\Big/D_r, \quad D_r = (1 - \frac{h}{2}\frac{\beta^+_x}{\beta^+}).$$

To obtain the higher-order approximate of $\frac{\partial u}{\partial x}\Big|^+$, it is necessary to handle the third- and fourth-order derivatives in (2.12). From (2.4) and (2.5), the expressions of u^+_{xxx} and u^+_{xxxx} can be given as

$$u^+_{xxx} = \Phi^+_1 u^+_x + \Phi^+_2 u^+ + \Phi^+_3, \tag{2.16}$$

and

$$u^+_{xxxx} = \Psi^+_1 u^+_x + \Psi^+_2 u^+ + \Psi^+_3, \tag{2.17}$$

where

$$\Phi^+_1 = -\frac{\beta^+_x}{\beta^+}\phi^+_1 + \phi^+_2, \quad \Phi^+_2 = \frac{c^+}{\beta^+}\phi^+_1 + \phi^+_3, \quad \Phi^+_3 = (-\frac{c^+}{\beta^+}\phi^+_1 + \phi^+_4)f^+ + \phi^+_5 f^+_x,$$
$$\Psi^+_1 = -\frac{\beta^+_x}{\beta^+}\psi^+_1 + \psi^+_2, \quad \Psi^+_2 = \frac{c^+}{\beta^+}\psi^+_1 + \psi^+_3, \quad \Psi^+_3 = \frac{f^+}{\beta^+}\psi^+_1 + \psi^+_4.$$

Keeping the first three terms on the right-hand side of (2.12), we establish the third-order accurate approximate of $\frac{\partial u}{\partial x}\Big|^+$ as follows:

$$\frac{\partial u}{\partial x}\Big|^+ = \bar{\rho}_{r,1}u^+ + \bar{\rho}_{r,2}u_{k+1} + \bar{\rho}_{r,3} + O(h^3), \tag{2.18}$$

where

$$\begin{aligned}\bar{\rho}_{r,1} &= -\left(\frac{1}{h} + \frac{h}{2}\frac{c^+}{\beta^+} + \frac{h^2}{6}\Phi^+_2\right)/\bar{D}_r, \quad \bar{\rho}_{r,2} = \frac{1}{h}/\bar{D}_r,\\ \bar{\rho}_{r,3} &= \left(\frac{h}{2}\frac{f^+}{\beta^+} - \frac{h^2}{6}\Phi^+_3\right)/\bar{D}_r, \quad \bar{D}_r = 1 - \frac{h}{2}\frac{\beta^+_x}{\beta^+} + \frac{h^2}{6}\Phi^+_1.\end{aligned}$$

Further, the fourth-order approximate of $\frac{\partial u}{\partial x}\Big|^+$ can be given as

$$\frac{\partial u}{\partial x}\Big|^+ = \bar{\bar{\rho}}_{r,1}u^+ + \bar{\bar{\rho}}_{r,2}u_{k+1} + \bar{\bar{\rho}}_{r,3} + O(h^4), \tag{2.19}$$

where

$$\begin{aligned}\bar{\bar{\rho}}_{r,1} &= -\left(\frac{1}{h} + \frac{h}{2}\frac{c^+}{\beta^+} + \frac{h^2}{6}\Phi^+_2 + \frac{h^3}{24}\Psi^+_2\right)/\bar{\bar{D}}_r, \quad \bar{\bar{\rho}}_{r,2} = \frac{1}{h}/\bar{\bar{D}}_r,\\ \bar{\bar{\rho}}_{r,3} &= \left(\frac{h}{2}\frac{f^+}{\beta^+} + \frac{h^2}{6}\Phi^+_3 + \frac{h^3}{24}\Psi^+_3\right)/\bar{\bar{D}}_r, \quad \bar{\bar{D}}_r = 1 - \frac{h}{2}\frac{\beta^+_x}{\beta^+} - \frac{h^2}{6}\Phi^+_1 + \frac{h^3}{24}\Psi^+_1.\end{aligned}$$

Similarly, the second-, third- and fourth-order approximation of $\frac{\partial u}{\partial x}\Big|^-$ can be given as

$$\frac{\partial u}{\partial x}\Big|^- = \rho_{l,1}u^- + \rho_{l,2}u_{k-1} + \rho_{l,3} + O(h^2), \tag{2.20}$$

$$\frac{\partial u}{\partial x}\Big|^- = \bar{\rho}_{l,1}u^- + \bar{\rho}_{l,2}u_{k-1} + \bar{\rho}_{l,3} + O(h^3), \tag{2.21}$$

$$\frac{\partial u}{\partial x}\Big|^- = \bar{\bar{\rho}}_{l,1}u^- + \bar{\bar{\rho}}_{l,2}u_{k-1} + \bar{\bar{\rho}}_{l,3} + O(h^4), \tag{2.22}$$

where

$$\rho_{l,1} = (\frac{1}{h} + \frac{h}{2}\frac{c^-}{\beta^-})\Big/D_l, \quad \rho_{l,2} = -\frac{1}{h}\Big/D_l, \quad \rho_{l,3} = -\frac{h}{2}\frac{f^-}{\beta^-}\Big/D_l, \quad D_l = 1 + \frac{h}{2}\frac{\beta^-_x}{\beta^-},$$

$$\begin{aligned}
\bar{\rho}_{l,1} &= \left(\frac{1}{h}+\frac{h}{2}\frac{c^-}{\beta^-}-\frac{h^2}{6}\Phi_2^-\right)/\bar{D}_l, \quad \bar{\rho}_{l,2}=-\frac{1}{h}/\bar{D}_l,\\
\bar{\rho}_{l,3} &= \left(-\frac{h}{2}\frac{f^-}{\beta^-}-\frac{h^2}{6}\Phi_3^-\right)/\bar{D}_l, \quad \bar{D}_l=1+\frac{h}{2}\frac{\beta_x^-}{\beta^-}+\frac{h^2}{6}\Phi_1^-,\\
\bar{\bar{\rho}}_{l,1} &= \left(\frac{1}{h}+\frac{h}{2}\frac{c^-}{\beta^-}-\frac{h^2}{6}\Phi_2^-+\frac{h^3}{24}\Psi_2^-\right)/\bar{\bar{D}}_l, \quad \bar{\bar{\rho}}_{l,2}=-\frac{1}{h}/\bar{\bar{D}}_l,\\
\bar{\bar{\rho}}_{l,3} &= \left(-\frac{h}{2}\frac{f^-}{\beta^-}+\frac{h^2}{6}\Phi_3^-+\frac{h^3}{24}\Psi_3^-\right)/\bar{\bar{D}}_l, \quad \bar{\bar{D}}_l=1+\frac{h}{2}\frac{\beta_x^-}{\beta^-}-\frac{h^2}{6}\Phi_1^-+\frac{h^3}{24}\Psi_1^-.
\end{aligned}$$

2.2. *Interface unfitted with mesh*

When the interface is located within one of the computational mesh, it appears as shown in Figure 3. The irregular nodes are k and $k+1$, and the construction of the higher order scheme is more complicated. Owing to the interface arbitrarily cutting through the computational mesh, the computational mesh of these irregular nodes is nonuniform, as shown in Figure 4.

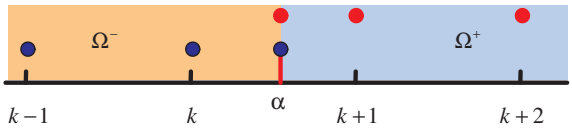

Figure 3. Interface unfitted with a body.

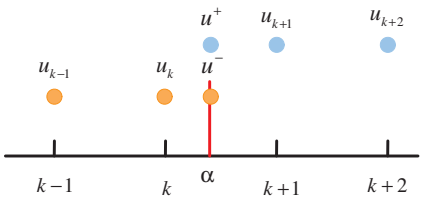

Figure 4. Nonuniform mesh.

We assume the function $u(x)$ is smooth enough, expand the $u(x_{i+1}), u(x_{i-1})$ at point x_i by Taylor series

$$\begin{aligned}
u_{i+1} &= u_i + h_f\frac{\partial u}{\partial x}\Big|_i + \frac{h_f^2}{2!}\frac{\partial^2 u}{\partial x^2}\Big|_i + \frac{h_f^3}{3!}\frac{\partial^3 u}{\partial x^3}\Big|_i + \frac{h_f^4}{4!}\frac{\partial^4 u}{\partial x^4}\Big|_i\\
&+ \frac{h_f^5}{5!}\frac{\partial^5 u}{\partial x^5}\Big|_i + O(h_f^6),
\end{aligned} \tag{2.23}$$

and

$$\begin{aligned}
u_{i-1} &= u_i - h_b\frac{\partial u}{\partial x}\Big|_i + \frac{h_b^2}{2!}\frac{\partial^2 u}{\partial x^2}\Big|_i - \frac{h_b^3}{3!}\frac{\partial^3 u}{\partial x^3}\Big|_i + \frac{h_b^4}{4!}\frac{\partial^4 u}{\partial x^4}\Big|_i\\
&- \frac{h_b^5}{5!}\frac{\partial^5 u}{\partial x^5}\Big|_i + O(h_b^6).
\end{aligned} \tag{2.24}$$

From (2.23) and (2.24), we can obtain

$$\begin{aligned}\frac{\partial^2 u}{\partial x^2}\Big|_i &= 2\frac{h_b u_{i+1} + h_f u_{i-1} - (h_f + h_b)u_i}{h_f h_b (h_f + h_b)} - \frac{h_f - h_b}{3}\frac{\partial^3 u}{\partial x^3}\Big|_i - \frac{1}{12}\frac{h_f^3 + h_b^3}{h_f + h_b}\frac{\partial^4 u}{\partial x^4}\Big|_i \\ &- \frac{1}{60}(h_f^2 + h_b^2)(h_f + h_b)\frac{\partial^5 u}{\partial x^5}\Big|_i + O(\frac{h_f^5 + h_b^5}{h_f + h_b}),\end{aligned} \tag{2.25}$$

and

$$\begin{aligned}\frac{\partial u}{\partial x}\Big|_i &= \frac{h_b^2 u_{i+1} - h_f^2 u_{i-1} + (h_f^2 - h_b^2)u_i}{h_b^2 h_f + h_f^2 h_b} - \frac{h_f h_b}{6}\frac{\partial^3 u}{\partial x^3}\Big|_i - \frac{h_f h_b (h_f - h_b)}{24}\frac{\partial^4 u}{\partial x^4}\Big|_i \\ &+ O(\frac{(h_f^3 + h_b^3)h_f h_b}{h_f + h_b}).\end{aligned} \tag{2.26}$$

Define the difference operators

$$\delta_x u_i = \frac{h_b^2 u_{i+1} - h_f^2 u_{i-1} + (h_f^2 - h_b^2)u_i}{h_b^2 h_f + h_f^2 h_b}, \tag{2.27}$$

$$\delta_x^2 u_i = 2\frac{h_b u_{i+1} + h_f u_{i-1} - (h_f + h_b)u_i}{h_f h_b (h_f + h_b)}. \tag{2.28}$$

Equations (2.25) and (2.26) can be rewritten as

$$\begin{aligned}\frac{\partial^2 u}{\partial x^2}\Big|_i &= \delta_x^2 u_i - \frac{h_f - h_b}{3}\frac{\partial^3 u}{\partial x^3}\Big|_i - \frac{1}{12}\frac{h_f^3 + h_b^3}{h_f + h_b}\frac{\partial^4 u}{\partial x^4}\Big|_i \\ &- \frac{1}{60}(h_f^2 + h_b^2)(h_f + h_b)\frac{\partial^5 u}{\partial x^5}\Big|_i + O(\frac{h_f^5 + h_b^5}{h_f + h_b}),\end{aligned} \tag{2.29}$$

and

$$\frac{\partial u}{\partial x}\Big|_i = \delta_x u_i - \frac{h_f h_b}{6}\frac{\partial^3 u}{\partial x^3}\Big|_i - \frac{h_f h_b (h_f - h_b)}{24}\frac{\partial^4 u}{\partial x^4}\Big|_i + O(\frac{(h_f^3 + h_b^3)h_f h_b}{h_f + h_b}). \tag{2.30}$$

Substituting Eqs (2.29) and (2.30) into the governing equation (1.1), we can get the difference scheme for the elliptic interface equation

$$-\beta\delta_x^2 u_i - \beta_x \delta_x u_i + k_i u_i + \tau = f_i, \tag{2.31}$$

where

$$\tau = Q_1\frac{\partial^3 u}{\partial x^3}\Big|_i + Q_2\frac{\partial^4 u}{\partial x^4}\Big|_i + Q_3\frac{\partial^5 u}{\partial x^5}\Big|_i + O(h^4), \tag{2.32}$$

and

$$Q_1 = \beta\frac{h_f - h_b}{3} - \beta_x\frac{h_f h_b}{6}, \quad Q_2 = \beta\frac{1}{12}\frac{h_f^3 + h_b^3}{h_f + h_b} - \beta_x\frac{h_f h_b (h_f - h_b)}{24},$$

$$Q_3 = \beta\frac{1}{60}(h_f^2 + h_b^2)(h_f + h_b).$$

To obtain the higher-order accuracy discrete scheme, it is necessary to handle the third- and fourth-order derivatives of the term τ. Substituting (2.4) and (2.5) into (2.31) and rearranging it, we have

$$\mathcal{A}_i\delta_x^2 u_i + \mathcal{B}\delta_x u_i + C_i u_i = \mathcal{F}_i + O((h_f^2 + h_b^2)(h_f + h_b)), \tag{2.33}$$

where

$$\mathcal{A}_i = -\beta + Q_1\phi_1 + Q_2\psi_1, \quad \mathcal{B}_i = -\beta_x + Q_1\phi_2 + Q_2\psi_2,$$
$$C_i = c_i + Q_1\phi_3 + Q_2\psi_3, \quad \mathcal{F}_i = f_i - Q_1(\phi_4 f_i + \phi_5 f_{x,i}) - Q_2\psi_4.$$

For the irregular points k and $k+1$, we use the interface α as one of the points in the compact stencil as shown in Figure 5. Thus, the 3-point compact stencil for nodes k and $k+1$ are $k-1, k, \alpha^-$ and $\alpha^+, k+1, k+2$, respectively. From the above analysis, the difference operators for the first- and second-order derivatives for nodes k and $k+1$ are respectively as follows

$$\delta_x u_k = \frac{h_b^2 u^- - h_f^2 u_{k-1} + (h_f^2 - h_b^2)u_k}{h_b^2 h_f + h_f^2 h_b}, \quad \delta_x^2 u_k = 2\frac{h_b u^- + h_f u_{k-1} - (h_f + h_b)u_k}{h_f h_b (h_f + h_b)}, \tag{2.34}$$

and

$$\delta_x u_{k+1} = \frac{h_b^2 u_{k+2} - h_f^2 u^+ + (h_f^2 - h_b^2)u_{k+1}}{h_b^2 h_f + h_f^2 h_b}, \quad \delta_x^2 u_{k+1} = 2\frac{h_b u_{k+2} + h_f u^+ - (h_f + h_b)u_{k+1}}{h_f h_b (h_f + h_b)}. \tag{2.35}$$

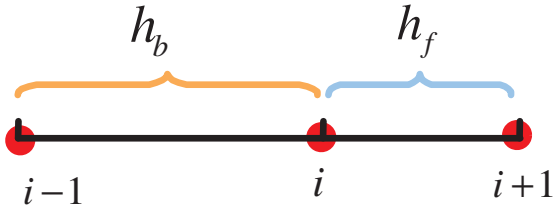

Figure 5. Stencil of interface unfitted with a body.

Substituting (2.34) and (2.35) into (2.33), we can get the higher-order compact scheme for the irregular point k:

$$\bar{A}_k u_{k-1} + \bar{B}_k u_k + \bar{C}_k u^- = \bar{F}_k + O((h_f^2 + h_b^2)(h_f + h_b)), \tag{2.36}$$

where

$$\bar{A}_k = \frac{2}{h_b(h_f + h_b)}\mathcal{A}_k - \frac{h_f^2}{h_b^2 h_f + h_f^2 h_b}\mathcal{B}_k, \quad \bar{B}_k = -\frac{2}{h_f h_b}\mathcal{A}_k + \frac{h_f^2 - h_b^2}{h_b^2 h_f + h_f^2 h_b}\mathcal{B}_k + C_k,$$
$$\bar{C}_k = \frac{2}{h_f(h_f + h_b)}\mathcal{A}_k + \frac{h_b^2}{h_b^2 h_f + h_f^2 h_b}\mathcal{B}_k, \quad \bar{F}_k = \mathcal{F}_k.$$

Similarly, the higher-order compact scheme for the irregular point $k+1$ is as follows:

$$\bar{A}_{k+1}u^{+} + \bar{B}_{k+1}u_{k+1} + \bar{C}_{k+1}u_{k+2} = \bar{F}_{k+1} + O((h_f^2 + h_b^2)(h_f + h_b)), \tag{2.37}$$

where

$$\begin{aligned}
\bar{A}_{k+1} &= \frac{2}{h_b(h_f+h_b)}\mathcal{A}_{k+1} - \frac{h_f^2}{h_b^2 h_f + h_f^2 h_b}\mathcal{B}_{k+1},\\
\bar{B}_{k+1} &= -\frac{2}{h_f h_b}\mathcal{A}_{k+1} + \frac{h_f^2 - h_b^2}{h_b^2 h_f + h_f^2 h_b}\mathcal{B}_{k+1} + C_{k+1},\\
\bar{C}_{k+1} &= \frac{2}{h_f(h_f+h_b)}\mathcal{A}_{k+1} + \frac{h_b^2}{h_b^2 h_f + h_f^2 h_b}\mathcal{B}_{k+1}, \quad \bar{F}_{k+1} = \mathcal{F}_{k+1}.
\end{aligned}$$

From the above analysis, we have constructed the higher-order compact scheme at regular points and irregular points. It should be noted that there are two auxiliary unknown quantities u^+ and u^- in the scheme for the irregular points k and $k+1$. Therefore, we have to find a way to deal with the interface connection conditions, so as to obtain a high-precision approximation for the auxiliary unknowns u^+ and u^- on both sides of the interface.

3. Approximation of the normal derivative on the interface

The first order derivative on both sides of the interface, $\frac{\partial u}{\partial x}\Big|^{+}$ and $\frac{\partial u}{\partial x}\Big|^{-}$, can respectively be given as

$$\begin{aligned}
\frac{\partial u}{\partial x}\Big|^{+} &= \frac{u_{k+1}-u^{+}}{h_{r1}} - \frac{h_{r1}}{2!}\frac{\partial^2 u}{\partial x^2}\Big|^{+} - \frac{h_{r1}^2}{3!}\frac{\partial^3 u}{\partial x^3}\Big|^{+} - \frac{h_{r1}^3}{4!}\frac{\partial^4 u}{\partial x^4}\Big|^{+}\\
&- \frac{h_{r1}^4}{5!}\frac{\partial^5 u}{\partial x^5}\Big|^{+} + O(h_r^5),
\end{aligned} \tag{3.1}$$

and

$$\begin{aligned}
\frac{\partial u}{\partial x}\Big|^{-} &= \frac{u^{-}-u_k}{h_{l1}} + \frac{h_{l1}}{2!}\frac{\partial^2 u}{\partial x^2}\Big|^{-} - \frac{h_{l1}^2}{3!}\frac{\partial^3 u}{\partial x^3}\Big|^{-} + \frac{h_{l1}^3}{4!}\frac{\partial^4 u}{\partial x^4}\Big|^{-}\\
&- \frac{h_{l1}^4}{5!}\frac{\partial^5 u}{\partial x^5}\Big|^{-} + O(h_l^5),
\end{aligned} \tag{3.2}$$

where $h_{l1} = \alpha - x_k$, $h_{r1} = x_{k+1} - \alpha$, $h_{l2} = h_{l1} + h$ and $h_{r2} = h_{r1} + h$, as shown in Figure 6.

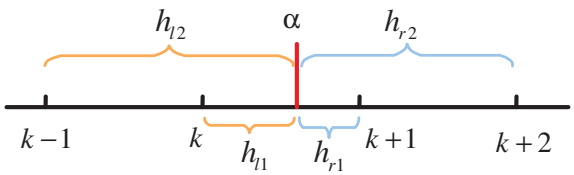

Figure 6. Interface and the irregular nodes.

Further, the second-order derivative on both sides of the interface, $\frac{\partial^2 u}{\partial x^2}\Big|^+$ and $\frac{\partial^2 u}{\partial x^2}\Big|^-$, can respectively be given as

$$\begin{aligned}\frac{\partial^2 u}{\partial x^2}\Big|^+ &= \frac{-2}{h_{r1}h_{r2}h}\left(h_{r2}u_{k+1} - h_{r1}u_{k+2} - hu^+\right) - \frac{h_{r1}+h_{r2}}{3}\frac{\partial^3 u}{\partial x^3}\Big|^+ \\ &- \frac{h_{r1}^2 + h_{r1}h_{r2} + h_{r2}^2}{12}\frac{\partial^4 u}{\partial x^4}\Big|^+ + O(h_{r1}^3 + h_{r2}^2 h_{r1} + h_{r1}^2 h_{r2} + h_{r2}^3),\end{aligned} \tag{3.3}$$

and

$$\begin{aligned}\frac{\partial^2 u}{\partial x^2}\Big|^- &= \frac{-2}{h_{l1}h_{l2}h}\left(h_{l2}u_{k} - h_{l1}u_{k-1} - hu^-\right) + \frac{h_{l1}+h_{l2}}{3}\frac{\partial^3 u}{\partial x^3}\Big|^- \\ &- \frac{h_{l1}^2 + h_{l1}h_{l2} + h_{l2}^2}{12}\frac{\partial^4 u}{\partial x^4}\Big|^- + O(h_{l1}^3 + h_{l2}^2 h_{l1} + h_{l1}^2 h_{l2} + h_{l2}^3).\end{aligned} \tag{3.4}$$

Substituting (3.3) and (3.4) into (3.1) and (3.2) respectively, we can get

$$\begin{aligned}\frac{\partial u}{\partial x}\Big|^+ &= \{-(\frac{1}{h_{r1}} + \frac{1}{h_{r2}})u^+ + (\frac{1}{h_{r1}} + \frac{1}{h})u_{k+1} - \frac{h_{r1}}{h_{r2}h}u_{k+2}\} + \frac{h_{r1}h_{r2}}{3!}\frac{\partial^3 u}{\partial x^3}\Big|^+ \\ &+ \frac{h_{r1}^2 h_{r2} + h_{r2}^2 h_{r1}}{4!}\frac{\partial^4 u}{\partial x^4}\Big|^+ + O(h_{r1}^3 + h_{r2}^2 h_{r1} + h_{r1}^2 h_{r2} + h_{r2}^3),\end{aligned} \tag{3.5}$$

and

$$\begin{aligned}\frac{\partial u}{\partial x}\Big|^- &= \{(\frac{1}{h_{l1}} + \frac{1}{h_{l2}})u^- - (\frac{1}{h_{l1}} + \frac{1}{h})u_k + \frac{h_{l1}}{h_{l2}h}u_{k-1}\} + \frac{h_{l1}h_{l2}}{3!}\frac{\partial^3 u}{\partial x^3}\Big|^+ \\ &- \frac{h_{l1}^2 h_{l2} + h_{l2}^2 h_{l1}}{4!}\frac{\partial^4 u}{\partial x^4}\Big|^+ + O(h_{l1}^3 + h_{l2}^2 h_{l1} + h_{l1}^2 h_{l2} + h_{l2}^3).\end{aligned} \tag{3.6}$$

3.1. Second-order scheme

Keep the first term in (3.6) and (3.5) and discard the other terms. We can get the approximation of the first order derivative on both sides of the interface with second-order accuracy:

$$u_x^- = \rho_{l,1}u^- + \rho_{l,2}u_k + \rho_{l,3}u_{k-1} + O(h^2), \tag{3.7}$$

and

$$u_x^+ = \rho_{r,1}u^+ + \rho_{r,2}u^{k+1} + \rho_{r,3}u_{k+2} + O(h^2), \tag{3.8}$$

where

$$\begin{aligned}\rho_{l,1} &= \frac{1}{h_{l1}} + \frac{1}{h_{l2}}, \quad \rho_{l,2} = -(\frac{1}{h_{l1}} + \frac{1}{h}), \quad \rho_{l,3} = \frac{h_{l1}}{hh_{l2}}, \\ \rho_{r,1} &= -(\frac{1}{h_{r1}} + \frac{1}{h_{r2}}), \quad \rho_{r,2} = \frac{1}{h_{r1}} + \frac{1}{h}, \quad \rho_{r,3} = -\frac{h_{r1}}{hh_{r2}}.\end{aligned}$$

3.2. Third-order scheme

Keeping the first two terms in (3.6) and (3.5) and discarding the other terms, and according to the (2.16), we can get the approximation of the first derivative with third order accuracy

$$u_x^- = \bar{\rho}_{l,1}u^- + \bar{\rho}_{l,2}u_k + \bar{\rho}_{l,3}u_{k-1} + \bar{\rho}_{l,4} + O(h^3), \tag{3.9}$$

and

$$u_x^+ = \bar{\rho}_{r,1}u^+ + \bar{\rho}_{r,2}u_{k+1} + \bar{\rho}_{r,3}u_{k+2} + \bar{\rho}_{r,4} + O(h^3), \tag{3.10}$$

where

$$\begin{aligned}
&\bar{\rho}_{l,1} = \left(\rho_{1,1} + \frac{h_{l1}h_{l2}}{6}\Phi_2^-\right)/\bar{D}_l, \quad \bar{\rho}_{l,2} = \rho_{1,2}/\bar{D}_l, \quad \bar{\rho}_{l,3} = \rho_{1,3}/\bar{D}_l,\\
&\bar{\rho}_{l,4} = \frac{h_{l1}h_{l2}}{6}\Phi_3^-/\bar{D}_l, \quad \bar{D}_l = 1 - \frac{h_{l1}h_{l2}}{6}\Phi_1^-,\\
&\bar{\rho}_{r,1} = \left(\rho_{r,1} + \frac{h_{r1}h_{r2}}{6}\Phi_2^+\right)/\bar{D}_r, \quad \bar{\rho}_{r,2} = \rho_{r,2}/\bar{D}_r, \quad \bar{\rho}_{r,3} = \rho_{r,3}/\bar{D}_r,\\
&\bar{\rho}_{l,4} = \frac{h_{r1}h_{r2}}{6}\Phi_3^+/\bar{D}_r, \quad \bar{D}_r = 1 - \frac{h_{r1}h_{r2}}{6}\Phi_1^+.
\end{aligned}$$

3.3. Fourth order scheme

Following the same manner as in the above subsection, we can get the approximation of the first derivative with fourth-order accuracy

$$u_x^- = \bar{\bar{\rho}}_{l,1}u^- + \bar{\bar{\rho}}_{l,2}u_k + \bar{\bar{\rho}}_{l,3}u_{k-1} + \bar{\bar{\rho}}_{l,4} + O(h^4), \tag{3.11}$$

and

$$u_x^+ = \bar{\bar{\rho}}_{r,1}u^+ + \bar{\bar{\rho}}_{r,2}u_{k+1} + \bar{\bar{\rho}}_{r,3}u_{k+2} + \bar{\bar{\rho}}_{r,4} + O(h^4), \tag{3.12}$$

where

$$\begin{aligned}
&\bar{\bar{\rho}}_{l,1} = \left(\rho_{l,1} + \frac{h_{l1}h_{l2}}{6}\Phi_2^- + \frac{h_{l2}^2h_{l1} + h_{l1}^2h_{l2}}{24}\Psi_2^-\right)/\bar{\bar{D}}_l, \quad \bar{\bar{\rho}}_{l,2} = \rho_{l,2}/\bar{\bar{D}}_l,\\
&\bar{\bar{\rho}}_{l,3} = \rho_{l,3}/\bar{\bar{D}}_l, \quad \bar{\bar{\rho}}_{l,4} = \left(\frac{h_{l1}h_{l2}}{6}\Phi_3^- + \frac{h_{l2}^2h_{l1} + h_{l1}^2h_{l2}}{24}\Psi_3^-\right)/\bar{\bar{D}}_l,\\
&\bar{\bar{\rho}}_{r,1} = \left(\rho_{r,1} - \frac{h_{l1}h_{l2}}{6}\Phi_1^- - \frac{h_{l2}^2h_{l1} + h_{l1}^2h_{l2}}{24}\Psi_1^-\right)/\bar{\bar{D}}_r, \quad \bar{\bar{\rho}}_{r,2} = \rho_{r,2}/\bar{\bar{D}}_r,\\
&\bar{\bar{\rho}}_{r,3} = \rho_{r,3}/\bar{\bar{D}}_r, \quad \bar{\bar{\rho}}_{r,4} = \left(\frac{h_{r1}h_{r2}}{6}\Phi_3^+ - \frac{h_{r2}^2h_{r1} + h_{r1}^2h_{r2}}{24}\Psi_3^+\right)/\bar{\bar{D}}_r,\\
&\bar{\bar{D}}_l = 1 - \frac{h_{l1}h_{l2}}{6}\Phi_1^- - \frac{h_{r2}^2h_{r1} + h_{r1}^2h_{r2}}{24}\Psi_1^+,\\
&\bar{\bar{D}}_r = 1 - \frac{h_{r1}h_{r2}}{6}\Phi_1^+ - \frac{h_{r2}^2h_{r1} + h_{r1}^2h_{r2}}{24}\Psi_1^+.
\end{aligned}$$

4. Compute u^+ and u^- on the interface

The implicit connecting condition on the interface is given as

$$\begin{cases} [u] = \lambda\beta^- u_x^-, \\ \beta^+ u_x^+ = \beta^- u_x^-. \end{cases} \tag{4.1}$$

For the interface fitted mesh, the approximation of the first-order derivative on both sides of the interface can respectively be written as

$$\frac{\partial u}{\partial x}\Big|^- = \rho_{l,1}u^- + \rho_{l,2}u_{k-1} + \rho_{l,3} + O(h_l^m), \tag{4.2}$$

$$\frac{\partial u}{\partial x}\Big|^+ = \rho_{r,1}u^+ + \rho_{r,2}u_{k+1} + \rho_{r,3} + O(h_r^m). \tag{4.3}$$

Discarding the terms $O(h_l^m)$ and $O(h_r^m)$ in (4.2) and (4.3), and substituting them into (4.1), the discrete format of the implicit connecting condition on the interface can be given as

$$\begin{cases} u^+ - u^- = \lambda\beta^-(\rho_{l,1}u^- + \rho_{l,2}u_{k-1} + \rho_{l,3}), \\ \beta^+(\rho_{r,1}u^+ + \rho_{r,2}u_{k+1} + \rho_{r,3}) = \beta^-(\rho_{l,1}u^- + \rho_{l,2}u_{k-1} + \rho_{l,3}). \end{cases}$$

For brevity, rearrange the above equation and establish linear equations with u^+ and u^- as variables as follows:

$$\begin{cases} a_{11}u^+ - a_{12}u^- = b_1, \\ a_{21}u^+ + a_{22}u^- = b_2, \end{cases}$$

where

$$\begin{aligned} &a_{11} = 1, \quad a_{12} = 1 + \lambda\beta^-\rho_{l,1}, \quad a_{21} = \beta^+\rho_{r,1}, \quad a_{22} = -\beta^-\rho_{l,1}. \\ &b_1 = \lambda\beta^-(\rho_{l,2}u_{k-1} + \rho_{l,3}), \\ &b_2 = \beta^-(\rho_{l,2}u_{k-1} + \rho_{l,3}) - \beta^+(\rho_{r,2}u_{k+1} + \rho_{r,3}). \end{aligned}$$

Solving the above linear system, we can get the approximate of each of the unknowns u^+ and u^- on both sides of the interface with m-th order accuracy:

$$u^+ = \tau_1^+ u_{k-1} + \tau_2^+ u_{k+1} + \tau_3^+, \tag{4.4}$$

$$u^- = \tau_1^- u_{k-1} + \tau_2^- u_{k+1} + \tau_3^-, \tag{4.5}$$

where

$$\begin{aligned} &\tau_1^+ = \frac{(a_{22}\lambda + a_{12})\beta^-\rho_{l,2}}{a_{11}a_{22} + a_{12}a_{21}}, \quad \tau_2^+ = -\frac{a_{12}\beta^+\rho_{r,2}}{a_{11}a_{22} + a_{12}a_{21}}, \\ &\tau_3^+ = \frac{(a_{22}\lambda + a_{12})\beta^-\rho_{l,3} - a_{12}\beta^+\rho_{r,3}}{a_{11}a_{22} + a_{12}a_{21}}, \end{aligned}$$

$$\tau_1^- = \frac{(a_{11} - a_{21}\lambda)\beta^-\rho_{l,2}}{a_{11}a_{22} + a_{12}a_{21}}, \quad \tau_2^- = -\frac{a_{11}\beta^+\rho_{r,2}}{a_{11}a_{22} + a_{12}a_{21}},$$
$$\tau_3^- = \frac{(a_{11} - a_{21}\lambda)\beta^-\rho_{l,3} - a_{11}\beta^+\rho_{r,3}}{a_{11}a_{22} + a_{12}a_{21}}.$$

For the interface-cut mesh, the approximation of the first-order derivative on both sides of the interface can be written as

$$\frac{\partial u}{\partial x}\Big|^- = \rho_{l,1}u^- + \rho_{l,2}u_k + \rho_{l,3}u_{k-1} + \rho_{l,4} + O(h_l^m), \tag{4.6}$$
$$\frac{\partial u}{\partial x}\Big|^+ = \rho_{r,1}u^+ + \rho_{r,2}u_{k+1} + \rho_{r,3}u_{k+2} + \rho_{r,4} + O(h_r^m). \tag{4.7}$$

In a similar manner as above, the approximate of each of the unknowns u^+ and u^- on both sides of the interface with m-th-order accuracy is given as

$$u^+ = \tau_1^+u_{k-1} + \tau_2^+u_k + \tau_3^+u_{k+1} + \tau_4^+u_{k+2} + \tau_5^+, \tag{4.8}$$
$$u^- = \tau_1^-u_{k-1} + \tau_2^-u_k + \tau_3^-u_{k+1} + \tau_4^-u_{k+2} + \tau_5^-, \tag{4.9}$$

where

$$\tau_1^+ = \frac{(a_{22}\lambda + a_{12})\beta^-\rho_{l,3}}{a_{11}a_{22} + a_{12}a_{21}}, \quad \tau_2^+ = \frac{(a_{22}\lambda + a_{12})\beta^-\rho_{l,2}}{a_{11}a_{22} + a_{12}a_{21}}, \quad \tau_3^+ = \frac{-a_{12}\beta^+\rho_{r,2}}{a_{11}a_{22} + a_{12}a_{21}},$$
$$\tau_4^+ = \frac{-a_{12}\beta^+\rho_{r,3}}{a_{11}a_{22} + a_{12}a_{21}}, \quad \tau_5^+ = \frac{a_{22}\lambda\beta^-\rho_{l,4} + a_{12}(\beta^-\rho_{l,4} - \beta^+\rho_{r,4})}{a_{11}a_{22} + a_{12}a_{21}},$$
$$\tau_1^- = \frac{(a_{11} - a_{21}\lambda)\beta^-\rho_{l,3}}{a_{11}a_{22} + a_{12}a_{21}}, \quad \tau_2^- = \frac{(a_{11} - a_{21}\lambda)\beta^-\rho_{l,2}}{a_{11}a_{22} + a_{12}a_{21}}, \quad \tau_3^- = \frac{-a_{11}\beta^+\rho_{r,2}}{a_{11}a_{22} + a_{12}a_{21}},$$
$$\tau_4^- = \frac{-a_{11}\beta^+\rho_{r,3}}{a_{11}a_{22} + a_{12}a_{21}}, \quad \tau_5^- = \frac{a_{11}(\beta^-\rho_{l,4} - \beta^+\rho_{r,4}) - a_{21}\lambda\beta^-\rho_{l,4}}{a_{11}a_{22} + a_{12}a_{21}}.$$

and

$$a_{11} = 1, \quad a_{12} = 1 + \lambda\beta^-\rho_{l,1}, \quad a_{21} = \beta^+\rho_{r,1}, \quad a_{22} = -\beta^-\rho_{l,1}.$$
$$b_1 = \lambda\beta^-(\rho_{l,2}u_k + \rho_{l,3}u_{k-1} + \rho_{l,4}),$$
$$b_2 = \beta^-(\rho_{l,2}u_k + \rho_{l,3}u_{k-1} + \rho_{l,4}) - \beta^+(\rho_{r,2}u_{k+1} + \rho_{r,3}u_{k+2} + \rho_{r,4}).$$

5. Discrete system

From the above sections, we establish the fourth-order compact finite-difference scheme for non-irregular mesh nodes:

$$A_iu_{i-1} + B_iu_i + C_iu_{i+1} = F_i, \tag{5.1}$$

for

$$i \neq \begin{cases} \{k-1, k+1\}, & \text{for body-fitted mesh,} \\ \{k, k+1\}, & \text{for non-body-fitted mesh.} \end{cases}$$

In the interface-fitted mesh case, the higher-order compact schemes at the irregular mesh nodes $k-1$ and $k+1$ are given as (2.7) and (2.8), respectively. Eliminating the auxiliary qualities u^+ and u^- by

substituting the formulas (4.4) and (4.5) into (2.7) and (2.8). The schemes for the irregular mesh nodes are given as

$$A_{k-1}u_{k-2} + B_{k-1}u_{k-1} + C_{k-1}u_{k+1} = F_{k-1}, \tag{5.2}$$

and

$$A_{k+1}u_{k-1} + B_{k+1}u_{k+1} + C_{k+1}u_{k+2} = F_{k+1}, \tag{5.3}$$

where

$$\begin{aligned}
&A_{k-1} = \bar{A}_{k-1}, \quad B_{k-1} = \bar{B}_{k-1} + \bar{C}_{k-1}\tau_1^-, \quad C_{k-1} = \bar{C}_{k-1}\tau_2^-,\\
&A_{k+1} = \bar{A}_{k+1}\tau_1^+, \quad B_{k+1} = \bar{B}_{k+1} + \bar{A}_{k+1}\tau_2^+, \quad C_{k+1} = \bar{C}_{k+1},\\
&F_{k-1} = \bar{F}_{k-1} - \bar{C}_{k-1}\tau_3^-, \quad F_{k+1} = \bar{F}_{k+1} - \bar{A}_{k+1}\tau_3^+.
\end{aligned}$$

Similarly, in the non-body-fitted case, the higher-order compact schemes at the irregular mesh nodes k and $k+1$ are respectively given as (2.36) and (2.37). Substitute the formulas (4.8) and (4.9) into (2.36) and (2.37) to eliminate the auxiliary qualities u^+ and u^-. The higher-order compact schemes at the irregular mesh nodes k and $k+1$ are respectively given as

$$A_k u_{k-1} + B_k u_k + C_k u_{k+1} + D_k u_{k+2} = F_k, \tag{5.4}$$

and

$$A_{k+1}u_{k-1} + B_{k+1}u_k + C_{k+1}u_{k+1} + D_{k+1}u_{k+2} = F_{k+1}, \tag{5.5}$$

where

$$\begin{aligned}
&A_k = \bar{A}_k + \bar{C}\tau_1^-, \quad B_k = \bar{B}_k + \bar{C}\tau_2^-, \quad C_k = \bar{C}_k\tau_3^-, \quad D_k = \bar{C}_k\tau_4^-,\\
&A_{k+1} = \bar{A}_{k+1}\tau_1^+, \quad B_{k+1} = \bar{A}_{k+1}\tau_2^+, \quad C_{k+1} = \bar{B}_{k+1} + \bar{A}_{k+1}\tau_3^+,\\
&D_{k+1} = \bar{C}_{k+1} + \bar{A}_{k+1}\tau_4^+, \quad F_k = \bar{F}_k - \bar{C}\tau_5^-, \quad F_{k+1} = \bar{F}_{k+1} - \bar{A}_{k+1}\tau_5^+.
\end{aligned}$$

Obviously, the resulting discrete linear equations have a tri-diagonal form for the body-fitted case and block-diagonal form for the non-body-fitted case, which can be efficiently solved by using existing numerical methods, such as the forward and backward sweep method, BiCGstab method, etc.

6. Numerical experiments

In this section, we use several numerical experiments to demonstrate the performance of the discrete schemes.

Example 1. Consider the computational domain $\Omega = [0, 1]$, and the solution is separated into two parts by the interface at $x = \alpha$,where $\alpha = 0.5$ and $\alpha = 0.52323$, for the interface-fitted mesh and interface-cut mesh cases, respectively. The analytical solution of this problem is given by

$$u(x, y) = \begin{cases} e^{x^2}, & x \in (0, \alpha), \\ \kappa e^{x^2}, & x \in (\alpha, 1). \end{cases}$$

The diffusion coefficient is defined as follows

$$\beta = \begin{cases} \kappa, & x \in (0, \alpha), \\ 1, & x \in (\alpha, 1). \end{cases}$$

Conservation of the flux on the interface satisfies

$$[\beta\frac{\partial u}{\partial x}] = \beta^{+}\frac{\partial u^{+}}{\partial x} - \beta^{-}\frac{\partial u^{-}}{\partial x} = 2\kappa x e^{x^2} - 2\kappa x e^{x^2} = 0, \quad at \quad x = \alpha.$$

The coefficient λ is given as

$$\lambda = \frac{\kappa e^{\alpha^2} - \alpha^2}{2\kappa\alpha e^{\alpha^2}}.$$

Tables 1 and 2 compare the L_2 and L_∞ errors in second-, third- and fourth-order formats on fitted and non-fitted mesh, respectively. The tables show that the numerical results of the three methods achieve theoretical accuracy on both fitted and non-fitted mesh.

Due to the strong discontinuity of physical quantities at the interface, it is crucial for the numerical scheme to be stable and robust. Tables 3 and 4 compare the errors of u^+ and u^- for different methods on fitted and non-fitted mesh, respectively. It can be seen from the tables that the physical quantities on both sides of the interface differ in magnitude by a factor of 100, but the numerical scheme proposed can capture the discontinuity of physical quantities on both sides of the interface with a high degree of accuracy.

Figure 7 compares the exact and numerical solutions on fitted and non-fitted mesh for Problem 1 at $k = 100$ with a number of intervals of 32. It is shown that the numerical solutions are well matched with the exact solutions, in spite of the fact that the amount of physical jumps on both sides of the interface are much larger. Figures 8 and 9 errors by the fourth-order, second-order and third-order scheme on fitted and non-fitted mesh, respectively. It can be seen that the errors are decrease as the number of mesh points increases.

Table 1. Comparison of L_2 and L_∞ errors in second-, third- and fourth-order formats on fitted mesh for Example 1, κ=100.

Mesh	Second-order scheme				Third-order scheme				Fourth-order scheme			
	L_2	Rate	L_∞	Rate	L_2	Rate	L_∞	Rate	L_2	Rate	L_∞	Rate
11	4.8e-1		8.7e-1		2.2e-2		4.7e-2		2.4e-3		4.5e-3	
21	1.2e-1	2.2	2.2e-1	2.1	2.4e-3	3.2	5.6e-3	3.1	1.4e-4	4.1	2.8e-4	4.0
41	2.8e-2	2.1	5.5e-2	2.0	2.8e-4	3.1	6.8e-4	3.0	8.8e-6	4.0	1.7e-5	4.0
81	6.9e-3	2.0	1.4e-2	2.0	3.4e-5	3.1	8.4e-5	3.0	5.4e-7	4.0	1.1e-6	4.0
161	1.7e-3	2.0	3.4e-3	2.0	4.2e-6	3.0	1.0e-5	3.0	3.3e-8	4.0	6.8e-8	4.0

Table 2. Comparison of L_2 and L_∞ errors in second-, third- and fourth-order formats on non-fitted mesh Example 1, κ=100.

Mesh	Second-order scheme				Third-order scheme				Fourth-order scheme			
	L_2	Rate	L_∞	Rate	L_2	Rate	L_∞	Rate	L_2	Rate	L_∞	Rate
11	8.9e-2		1.8e-1		9.8e-2		2.7e-1		2.4e-3		4.5e-3	
21	6.9e-2	0.4	1.2e-1	0.6	2.4e-2	2.0	4.5e-2	2.6	1.5e-4	4.0	2.8e-4	4.0
41	2.8e-2	1.3	5.5e-2	1.1	3.5e-3	2.8	7.3e-3	2.6	8.8e-6	4.0	1.8e-5	4.0
81	6.8e-3	2.2	1.3e-2	2.0	4.3e-4	3.1	8.4e-4	3.1	5.4e-7	4.0	1.1e-6	4.0
161	1.5e-3	2.1	3.0e-3	2.2	5.5e-5	2.9	1.0e-4	3.0	3.4e-8	4.0	6.8e-8	5.0

Table 3. Comparison of the errors of u^+ and u^- for different methods on fitted mesh for Example 1, κ=100.

		(u^-, u^+) = (1.284025, 128.4025)				
	Mesh	11	21	41	81	161
Second	e_∞	(8.6e-4, 8.7e-1)	(2.1e-4,2.2e-1)	(5.3e-5,5.5e-2)	(1.3e-5,1.4e-2)	(3.3e-6,3.4e-3)
	e_∞^{2h}/e_∞^h	-	(4.0,4.0)	(4.0,4.0)	(4.0, 4.0)	(4.0,4.0)
Third	e_∞	(8.6e-4,4.7e-2)	(1.1e-4,5.6e-3)	(1.4e-5, 6.8e-4)	(1.7e-6, 8.4e-5)	(2.1e-7, 1.0e-5)
	e_∞^{2h}/e_∞^h	-	(8.0, 8.4)	(7.9, 8.2)	(8.0,8.1)	(8.0, 8.1)
Fourth	e_∞	(1.2e-5,4.5e-3)	(7.3e-7,2.8e-4)	(4.6e-8, 1.8e-5)	(2.9e-9, 1.1e-6)	(1.8e-10,6.8e-8)
	e_∞^{2h}/e_∞^h	-	(15.9, 16.0)	(16.0,16.0)	(16.0, 16.1)	(16.1, 16.0)

Table 4. Comparison of the errors of u^+ and u^- for different methods on non-fitted mesh for Example 1, κ=100.

		(u^-, u^+) = (1.284025, 128.4025)				
	mesh	11	21	41	81	161
Second	e_∞	(4.7e-3, 1.3e-1)	(1.6e-3,1.1e-1)	(1.3e-3,5.5e-2)	(2.7e-4,1.3e-2)	(6.4e-5,3.0e-3)
	e_∞^{2h}/e_∞^h	-	(3.6,4.2)	(3.8,4.1)	(3.9, 4.1)	(4.2,4.5)
Third	e_∞	(8.7e-4,4.7e-2)	(1.1e-4,5.6e-3)	(1.4e-5, 6.8e-4)	(1.7e-6, 8.4e-5)	(2.1e-7, 1.0e-5)
	e_∞^{2h}/e_∞^h	-	(8.0, 8.4)	(7.9, 8.2)	(8.0,8.1)	(8.0, 8.1)
Fourth	e_∞	(1.2e-5,4.5e-3)	(7.3e-7,2.8e-4)	(4.6e-8, 1.8e-5)	(2.9e-9, 1.1e-6)	(1.8e-10,6.8e-8)
	e_∞^{2h}/e_∞^h	-	(15.9, 16.0)	(16.0,16.0)	(16.0, 16.1)	(16.1, 16.0)

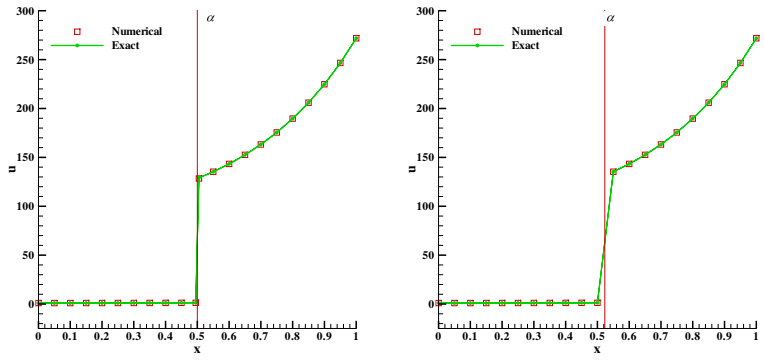

(a) Interface-fitted mesh (b) Interface-cut mesh

Figure 7. Comparison of exact and numerical solutions on fitted and non-fitted mesh for Problem 1.

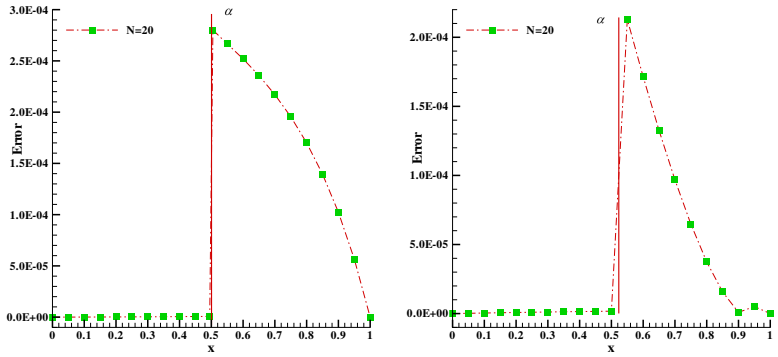

(a) Interface-fitted mesh (b) Interface-cut mesh

Figure 8. Comparison of errors by the fourth-order scheme on fitted mesh and non-fitted mesh for Example 1.

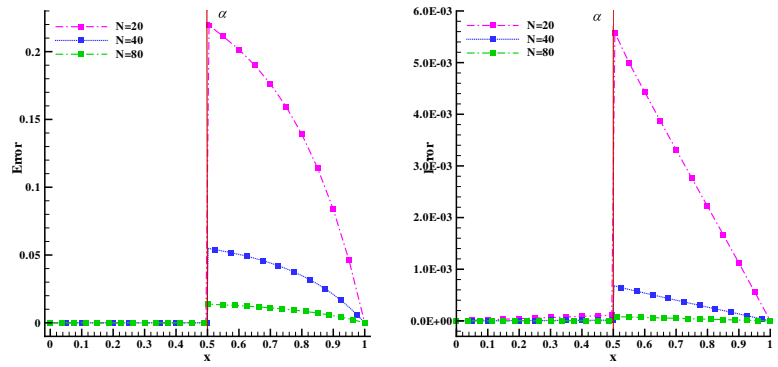

(a) Second-order scheme (b) Third-order scheme

Figure 9. Comparison of errors by the second-order and third-order schemes for Example 1.

Example 2. Consider the elliptic interface problem with a variable diffusion coefficient, and the solution is separated into two parts by the interface at $x = \alpha$, where $\alpha = 0.5$ and $\alpha = 0.53232$, for the interface-fitted mesh and interface-cut mesh cases, respectively. The analytical solution of this problem is given by

$$u(x, y) = \begin{cases} x^2 e^x, & x \in (0, \alpha), \\ \kappa e^x, & x \in (\alpha, 1). \end{cases}$$

The diffusion coefficient is defined as follows

$$\beta = \begin{cases} \kappa, & x \in (0, \alpha), \\ 2x + x^2, & x \in (\alpha, 1). \end{cases}$$

Conservation of the flux on the interface satisfies

$$[\beta \frac{\partial u}{\partial x}] = \beta^+ \frac{\partial u^+}{\partial x} - \beta^- \frac{\partial u^-}{\partial x} = \kappa(2x + x^2)e^x - \kappa(2x + x^2)e^x = 0, \quad at \quad x = \alpha.$$

The coefficient λ is given as

$$\lambda = \frac{\kappa - \alpha^2}{\kappa(2\alpha + \alpha^2)}.$$

Tables 5 and 6 compare the L_2 and L_∞ errors in second-, third- and fourth-order formats on fitted and non-fitted mesh, respectively. It can be seen that the numerical format is able to achieve theoretical accuracy on fitted mesh. The numerical accuracy on the non-fitted mesh is slightly lower than the theoretical accuracy, probably due to the unbalanced grid step on both sides of the interface, which leads to the instability of the format.

Figure 10 compares the exact and numerical solutions on fitted and non-fitted mesh for Problem 1 at $k = 100$ with a number of intervals of 41. It is shown that the numerical solutions are well matched with the exact solutions, in spite of the fact that the amount of physical jumps on both sides of the interface are much larger. Figure 11 compares errors by the fourth-order and third-order schemes on fitted and non-fitted mesh, respectively. As seen in the table, the errors in the fourth-order scheme are significantly lower than those in the third-order scheme.

Table 5. Comparison of L_2 and L_∞ errors in second-, third- and fourth-order formats on fitted mesh for Example 2, κ=100.

Mesh	Second-order scheme				Third-order scheme				Fourth-order scheme			
	L_2	Rate	L_∞	Rate	L_2	Rate	L_∞	Rate	L_2	Rate	L_∞	Rate
21	1.4e-2		2.9e-2		9.9e-5		2.4e-4		3.2e-6		6.1e-6	
41	3.4e-3	2.0	7.3e-3	2.0	1.1e-5	3.1	2.9e-5	3.1	2.0e-7	4.0	4.0e-7	4.0
81	8.3e-4	2.0	1.8e-3	2.0	1.4e-6	3.1	3.5e-6	3.0	1.2e-8	4.0	2.5e-8	4.0
161	2.1e-4	2.0	4.6e-4	2.0	1.7e-7	3.0	4.3e-7	3.0	7.5e-10	4.0	1.5e-9	4.1
321	5.1e-5	2.0	1.1e-4	2.0	2.1e-8	3.0	5.4e-8	3.0	4.6e-11	4.0	9.2e-11	4.1

Table 6. Comparison of L_2 and L_∞ errors in second-, third- and fourth-order formats on non-fitted mesh for Example 2, κ=100.

Mesh	Second-order scheme				Third-order scheme				Fourth-order scheme			
	L_2	Rate	L_∞	Rate	L_2	Rate	L_∞	Rate	L_2	Rate	L_∞	Rate
21	8.9e-3		1.5e-2		1.3e-3		5.9e-3		1.1e-3		5.2e3	
41	3.6e-3	1.3	7.6e-3	1.0	3.2e-5	5.3	7.5e-5	6.3	3.2e-5	5.1	8.8e-5	5.9
81	8.3e-4	2.1	1.8e-3	2.1	3.7e-6	3.1	1.3e-5	2.5	3.8e-6	3.1	1.5e-5	2.6
161	1.8e-4	2.2	4.0e-4	2.2	4.2e-7	3.1	3.8e-6	1.8	4.8e-7	3.0	4.0e-6	1.9
321	2.8e-5	2.7	5.2e-5	2.9	9.5e-8	2.2	1.7e-6	1.2	9.9e-8	2.3	1.7e-6	1.3

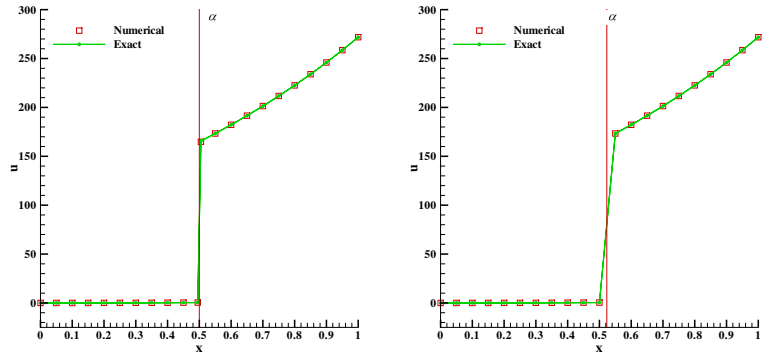

(a) Interface-fitted mesh (b) Interface-cut mesh

Figure 10. Comparison of exact and numerical solutions for Problem 2.

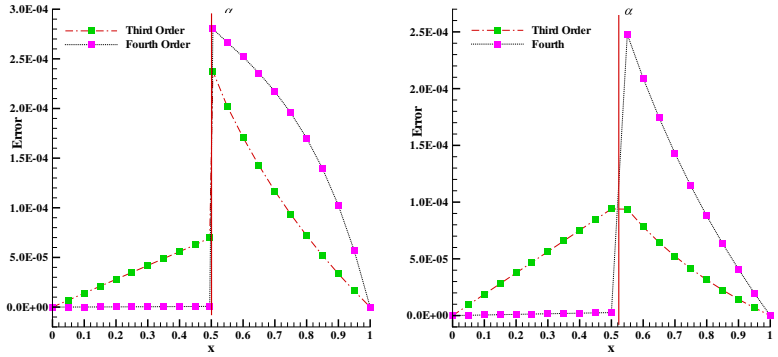

(a) Interface-fitted mesh (b) Interface-cut mesh

Figure 11. Comparison of errors under different kinds schemes for Problem 2.

Table 7 compares the length ratio of the interface-cut mesh interval. The table shows that as the number of grids changes, the spacing ratio changes significantly and affects the accuracy of the numerical scheme.

Table 7. Comparison of the length ratio h_f/h_b of interface-cut mesh.

Mesh	21	41	81	161	321
h_f/h_b	1.48	2.80	1.72e-2	1.36	2.30

Table 8 compares the condition numbers of the linear system matrix A for the fitted and non-fitted meshes. It can be seen that the condition number of the matrix does not differ much for the same grid number, so the proposed numerical scheme is stable.

Table 8. Comparison of condition numbers of the linear system on fitted and non-fitted mesh.

Mesh	21	41	81	161	321
Fitted	2098	6746	20081	63749	147695
Non-fitted	4108	14355	31339	107609	341350

Example 3. Consider the elliptic interface problem with a variable diffusion coefficient, and the solution is separated into two parts by the interface at $x = \alpha$, where $\alpha = 0.5$ and $\alpha = 0.53232$, for the interface-fitted mesh and interface-cut mesh cases, respectively. The analytical solution of this problem is given by

$$u(x, y) = \begin{cases} \sin x e^{x^2}, & x \in (0, \alpha), \\ \kappa e^{x^2}, & x \in (\alpha, 1). \end{cases}$$

The diffusion coefficient is defined as follows

$$\beta = \begin{cases} 2\kappa x, & x \in (0, \alpha), \\ \cos x + 2x \sin x, & x \in (\alpha, 1). \end{cases}$$

Conservation of the flux on the interface satisfies

$$[\beta \frac{\partial u}{\partial x}] = \beta^+ \frac{\partial u^+}{\partial x} - \beta^- \frac{\partial u^-}{\partial x} = 2\kappa x(2x \sin x + \cos x)e^{x^2} - 2\kappa x(2x \sin x + \cos x)e^{x^2} = 0.$$

The coefficient λ is given as

$$\lambda = \frac{\kappa - \sin \alpha}{2\kappa\alpha(\cos \alpha + 2\alpha \sin \alpha)}.$$

Tables 9 and 10 compare the L_2 and L_∞ errors in second-, third- and fourth-order formats on fitted and non-fitted mesh, respectively. It is shows that the numerical format is able to achieve theoretical accuracy on fitted mesh.

Figure 12 compares the exact and numerical solutions on fitted and non-fitted mesh for Problem 1 at $k = 100$ with a number of intervals of 41. It can be seen that the error in matching the numerical solution to the exact solution is essentially small despite the large physical jumps on both sides of the interface. Figure 13 compares errors by the fourth-order and third-order schemes on fitted and non-fitted mesh, respectively. As can be seen in the table, the numerical accuracy of the fourth-order scheme is better than that of the third-order scheme.

Table 9. Comparison of L_2 and L_{infty} errors in second-, third- and fourth-order formats on fitted mesh for Example 3, κ=1000.

Mesh	Second-order scheme				Third-order scheme				Fourth-order scheme			
	L_2	Rate	L_∞	Rate	L_2	Rate	L_∞	Rate	L_2	Rate	L_∞	Rate
21	1.4		2.6		2.1e-2		5.0e-2		1.8e-3		3.4e-3	
41	3.4e-1	2.0	6.4e-1	2.0	2.4e-3	3.1	6.0e-3	3.1	1.1e-4	4.0	2.1e-4	4.0
81	8.4e-2	2.0	1.6e-1	2.0	2.9e-4	3.1	7.4e-4	3.0	6.9e-6	4.0	1.3e-5	4.0
161	2.1e-2	2.0	4.0e-2	2.0	3.5e-5	3.0	9.1e-5	3.0	4.4e-7	4.0	8.5e-7	4.0
321	5.2e-3	2.0	1.0e-2	2.0	4.3e-6	3.0	1.1e-5	3.0	2.9e-8	3.9	5.5e-8	3.9

Table 10. Comparison of L_2 and L_{infty} errors in second-, third- and fourth-order formats on non-fitted mesh for Example 3, κ=1000.

Mesh	Second-order scheme				Third-order scheme				Fourth-order scheme			
	L_2	Rate	L_∞	Rate	L_2	Rate	L_∞	Rate	L_2	Rate	L_∞	Rate
21	9.9e-1		1.7		4.0e-2		1.4e-1		1.4e-2		6.3e-2	
41	3.4e-1	1.6	6.4e-1	1.4	8.2e-4	5.6	1.9e-3	6.2	1.1e-3	3.7	2.5e-3	4.6
81	8.1e-2	2.1	1.6e-1	2.0	5.3e-5	4.0	1.2e-4	4.0	1.1e-4	3.2	2.9e-4	3.1
161	1.9e-2	2.1	3.6e-2	2.1	1.0e-5	2.4	5.9e-5	1.0	1.1e-5	3.3	3.0e-5	3.3
321	3.6e-3	2.4	6.3e-3	2.5	1.8e-6	2.5	3.9e-5	0.6	1.2e-6	3.3	1.7e-6	4.1

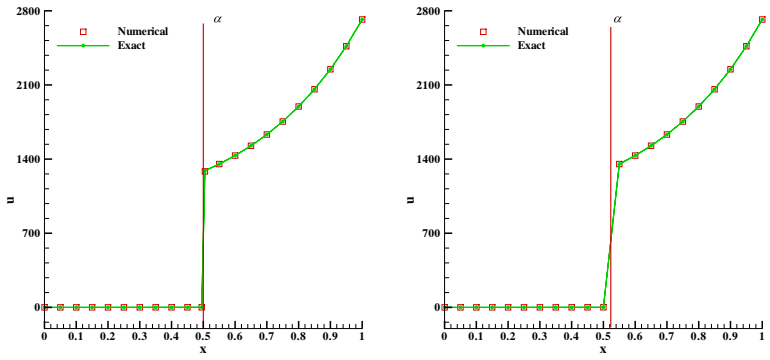

(a) Interface-fitted mesh (b) Interface-cut mesh

Figure 12. Comparison of exact and numerical solutions for Problem 3.

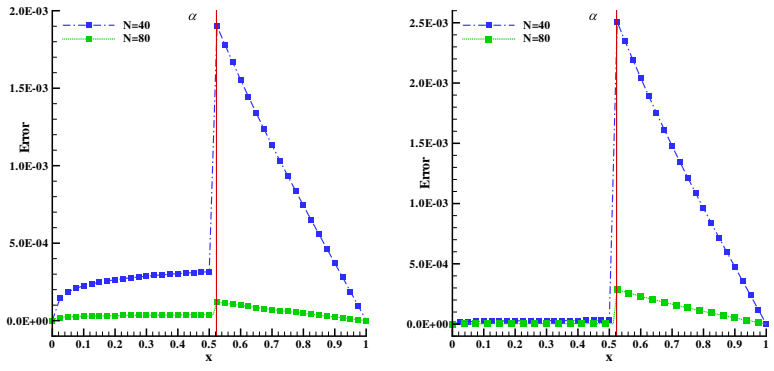

(a) Third-order scheme (b) Fourth-order scheme

Figure 13. Errors under the third-order scheme (a) and fourth-order scheme (b) for Problem 3, with different mesh sizes.

7. Conclusions

The 1D elliptic interface problem with imperfect contact is characterized by the fact that the jump quantity of the solution is unknown and is related to the flux across the interface. In this paper, a class of higher-order finite-difference schemes is constructed for interface fitted and non-fitted meshes, respectively. The second-, third-, and fourth-order approximations of the jump conditions are provided by using the connected jump conditions and their higher-order derivatives. Some numerical experiments were carried out to illustrate the accuracy and stability of the present method. The numerical results show that the proposed scheme is able to capture the solution of the discontinuous case of the interface body with theoretical accuracy. The theoretical accuracy has been achieved for the elliptic interface problem with implicit interface connection conditions.

Acknowledgments

This work was partly supported by the National Natural Science Foundation (12161067, 12261067, 12001015, 62201298, 51961031), the National Natural Science Foundation of China Youth Fund Project (11801287), the Inner Mongolia Autonomous Region Youth Science and Technology Talents Support Program (NJYT20B15), the Inner Mongolia Scientific Fund Project (2020MS06010, 2021LHMS01006, 2022MS01008), and Innovation Fund Project of Inner Mongolia University of Science and Technology-Excellent Youth Science Fund Project (2019YQL02).

Conflict of interest

The authors declare that the publication of this paper does coincide with any confilict of interest.

References

1. A. A. Samarskii, V. B. Andreev, *Differential method for elliptic equations [in Russian]*, Nauka, Moscow, 1976.
2. A. A. Samarskii, *The theroy of difference scheme*, Marcel Dekker, Inc., 2001.
3. A. A. Samarskii, P. N. Vabishchevich, *Computational heat transfer*, Vol. 1, John Wiley& Sons Ltd, 1995.
4. Z. Q. Huang , E. J. Ding, *Transport theory*, 2 Eds., Beijing: Science Press, 2008.
5. G. Lopez-Ruiz, J. Bravo-Castillero, R. Brenner, M. E. Cruzd, R. Guinovart-Díazb, L. D. Pérez-Fernándeze, et al., Variational bounds in composites with nonuniform interfacial thermal resistance, *Appl. Math. Model.*, **39** (2015), 7266–7276. https://doi.org/10.1016/j.apm.2015.02.048
6. R. P. A. Rocha, M. A. E. Cruz, Computation of the effective conductivity of unidirectional fibrous composites with an interfacial thermal resistance, *Numer. Heat Transfer, Part A*, **39** (2001), 179–203. https://doi.org/10.1080/10407780118981
7. R. Costa, J. M. Nobrega, S. Clain, G. J. Machado, Very high-order accurate polygonal mesh finite volume scheme for conjugate heat transfer problems with curved interfaces and imperfect contacts, *Comput. Methods Appl. Mech. Eng.*, **357** (2019), 112560. https://doi.org/10.1016/j.cma.2019.07.029

8. R. J. LeVeque, Z. L. Lin, The immersed interface method for elliptic equations with discontinuous coefficients and singular sources, *SIAM J. Numer. Anal.*, **31** (1994), 1019–1044. https://doi.org/10.1137/0731054
9. R. J. LeVeque, Z. L. Lin, Immersed interface methods for Stokes flow with elastic boundaries or surface tension, *SIAM J. Sci. Comput.*, **18** (1997), 709–735. https://doi.org/10.1137/S1064827595282532
10. Z. Li, M. C. Lai, The immersed interface method for the Navier-Stokes equations with singular forces, *J. Comput. Phys.*, **171** (2001), 822–842. https://doi.org/10.1006/jcph.2001.6813
11. K. Ito, Z. Li, Solving a nonlinear problem in magneto-rheological fluids using the immersed interface method, *J. Sci. Comput.*, **19** (2003), 253–266. https://doi.org/10.1023/A:1025356025745
12. Z. Li, K. Ito, Maximum principle preserving schemes for interface problems, *J. Sci. Comput.*, **23** (2001), 339–361. https://doi.org/10.1137/S1064827500370160
13. Z. Li, K. Ito, *The immersed interface method: numerical solutions of PDEs involving interfaces and irregular domains*, SIAM, Philadelphia, 2006.
14. A. Wiegmann, K. P. Bube, The immersed interface method for nonlinear differential equations with discontinuous coefficients and singular sources, *SIAM J. Numer. Anal.*, **35** (1998), 177–200. https://doi.org/10.1137/S003614299529378X
15. M. Colnago, W. Casaca, L. Franco de Souza, A high-order immersed interface method free of derivative jump conditions for Poisson equations on irregular domains, *J. Comput. Phys.*, **423** (2020), 109791, https://doi.org/10.1016/j.jcp.2020.109791
16. F. Gibou, R. Fedkiw, A fourth order accurate discretization for the laplace and heat equations on arbitrary domains, with applications to the stefan problem, *J. Computat. Phys.*, **202** (2005), 577–601. https://doi.org/10.1016/j.jcp.2004.07.018
17. H. Wu, High order scheme for Schrodinger equation with discontinuous potential I: immersed interface method, *Numer. Math.: Theory, Methods Appl.*, **4** (2011), 576–597. https://doi.org/10.1017/S100489790000074X
18. S. Abide, B. Zeghmati, Multigrid defect correction and fourth-order compact scheme for Poisson's equation, *Comput. Math. Appl.*, **73** (2017), 1433–1444. https://doi.org/10.1016/j.camwa.2017.01.016
19. S. Abide, Finite difference preconditioning for compact scheme discretizations of the Poisson equation with variable coefficients, *J. Comput. Appl. Math.*, **379** (2020), 112872. https://doi.org/10.1016/j.cam.2020.112872
20. R. P. Fedkiw, T. Aslam, B. Merriman, S. Osher, A non-oscillatory Eulerian approach to interfaces in multimaterial flows (the ghost fluid method), *J. Comput. Phys.*, **152** (1999), 457–492. https://doi.org/10.1006/jcph.1999.6236
21. X. D. Liu, R. P. Fedkiw, M. Kang, A boundary condition capturing method for Poisson equation on irregular domains, *J. Comput. Phys.*, **160** (2000), 151–178. https://doi.org/10.1006/jcph.2000.6444
22. M. Oevermann, C. Scharfenberg, R. Klein, A sharp interface finite volume method for elliptic equations on Cartesian grids, *J. Comput. Phys.*, **228** (2009), 5184–5206. https://doi.org/10.1016/j.jcp.2009.04.018

23. M. Oevermann, R. Klein, A cartesian grid finite volume method for elliptic equations with variable coefficients and embedded interfaces, *J. Comput. Phys.*, **219** (2006), 749–769. https://doi.org/10.1016/j.jcp.2006.04.010

24. F. Cao, Z. Sheng, G. Yuan, Monotone finite volume schemes for diffusion equation with imperfect interface on distorted meshes, *J. Sci. Comput.*, **76** (2018), 1055–1077. https://doi.org/10.1007/s10915-018-0651-8

25. Y. C. Zhou, S. Zhao, M. Feig, G. W. Wei, High order matched interface and boundary method for elliptic equations with discontinuous coefficients and singular sources, *J. Comput. Phys.*, **213** (2006), 1–30. https://doi.org/10.1016/j.jcp.2005.07.022

26. K. Xia, M. Zhan, G. W. Wei, MIB method for elliptic equations with multi-material interfaces, *J. Comput. Phys.*, **230** (2011), 4588–4615. https://doi.org/10.1016/j.jcp.2011.02.037

27. H. Feng, G. Long, S. Zhao, An augmented matched interface and boundary (MIB) method for solving elliptic interface problem, *J. Comput. Appl. Math.*, **361** (2019), 426–443. https://doi.org/10.1016/j.cam.2019.05.004

28. H. Wang, J. Chen, P. Sun, F. Qin, A conforming enriched finite element method for elliptic interface problems, *Appl. Numer. Math.: Trans. IMACS*, **127** (2018), 1–17. https://doi.org/10.1016/j.apnum.2017.12.011

29. G. Jo, D. Y. Kwak, Enriched P_1-conforming methods for elliptic interface problems with implicit jump conditions, *Adv. Math. Phys.*, **2018** (2018), 1–9. https://doi.org/10.1155/2018/9891281

30. L. Wang, S. Hou, L. Shi, A simple FEM for solving two-dimensional diffusion equation with nonlinear interface jump conditions, *Comput. Model. Eng. Sci.*, **119** (2019), 73–90. https://doi.org/10.32604/cmes.2019.04581

31. Y. Xiao, J. Xu, F. Wang, High-order extended finite element methods for solving interface problems, *Comput. Methods Appl. Mech. Eng.*, **364** (2020), 112964. https://doi.org/10.1016/j.cma.2020.112964

32. A. Loubenets, T. Ali, M. Hanke, Highly accurate finite element method for one-dimensional elliptic interface problems, *Appl. Numer. Math.*, **59** (2009), 119–134. https://doi.org/10.1016/j.apnum.2007.12.003

33. J. Guzman, M. A. Sanchez, M. Sarkis, Higher-order finite element methods for elliptic problems with interfaces, *ESAIM: Math. Model. Numer. Anal.*, **50** (2016), 1561–1583. https://doi.org/10.1051/m2an/2015093

34. T. Lin, D. Sheen, X. Zhang, A noncomforming immersed finite element method for elliptic interface problems, *J. Sci. Comput.*, **79** (2019), 442–463. https://doi.org/10.1007/s10915-018-0865-9

35. Q. Zhuang, R. Guo, High degree discontinuous Petrov-Galerkin immersed finite element methods using fictitious elements for elliptic interface problems, *J. Comput. Appl. Math.*, **362** (2019), 560–573. https://doi.org/10.1016/j.cam.2018.09.028

36. H. Ji, Z. Weng, Q. Zhang, An augmented immersed finite element method for variable coefficient elliptic interface problems in two and three dimensions, *J. Comput. Phys.*, **418** (2020), 109631. https://doi.org/10.1016/j.jcp.2020.109631

37. R. Guo, T. Lin, An immersed finite element method for elliptic interface problems in three dimensions, *J. Comput. Phys.*, **414** (2020), 109478. https://doi.org/10.1016/j.jcp.2020.109478
38. R. Guo, T. Lin, A higher degree immersed finite element method based on a cauchy extension for elliptic interface problems, *SIAM J. Numer. Anal.*, **57** (2019), 1545–1573. https://doi.org/10.1137/18M121318X
39. M. N. Linnick, H. F. Fasel, A high-order immersed interface method for simulating unsteady incompressible flows on irregular domains, *J. Comput. Phys.*, **204** (2004), 157–192. https://doi.org/10.1016/j.jcp.2004.09.017
40. X. Zhong, A new high-order immersed interface method for solving elliptic equations with imbedded interface of discontinuity, *J. Comput. Phys.*, **225** (2007), 1066–1099. https://doi.org/10.1016/j.jcp.2007.01.017
41. I. T. Angelova, L. G. Vulkov, High-order finite difference schemes for elliptic problems with intersecting interfaces, *Appl. Math. Comput.*, **187** (2007), 824–843. https://doi.org/10.1016/j.amc.2006.08.165
42. H. Feng, S. Zhao, A fourth order finite difference method for solving elliptic interface problems with the FFT acceleration, *J. Comput. Phys.*, **419** (2020), 109677, https://doi.org/10.1016/j.jcp.2020.109677
43. J. Li, J. M. Melenk, B. Wohlmuthc, J. Zou, Optimal a priori estimates for higher order finite elements for elliptic interface problems, *Appl. Numer. Math.*, **60** (2010), 19–37. https://doi.org/10.1016/j.apnum.2009.08.005
44. L. N. T. Huynh, N. C. Nguyen, J. Peraire, B. C. Khoo, A high-order hybridizable discontinuous Galerkin method for elliptic interface problems, *Int. J. Numer. Methods Eng.*, **93** (2013), 183–200. https://doi.org/10.1002/nme.4382
45. H. Huang, J. Li, J. Yan, High order symmetric direct discontinuous Galerkin method for elliptic interface problems with fitted mesh, *J. Comput. Phys.*, **409** (2020), 109301. https://doi.org/10.1016/j.jcp.2020.109301
46. Y. Xiao, J. Xu, F. Wang, High-order extended finite element methods for solving interface problems, *Comput. Methods Appl. Mech. Eng.*, **364** (2020), 112964. https://doi.org/10.1016/j.cma.2020.112964
47. M. M. Gupta, R. P. Manohar, J. W. Stephenson, High-order difference schemes for two-dimensional elliptic equations, *Numer. Methods Partial Differ. Equ.*, **1** (1985), 71–80. https://doi.org/10.1002/num.1690010108

AIMS Press